Materials Research. 2019; 22(suppl.2): e20180766
DOI: http://dx.doi.org/10.1590/1980-5373-MR-2018-0766

Effects of Gas Nitriding on Fatigue and Crack Initiation of Ti6Al4V produced by Selective Laser Melting

Aamir Mukhtar[a]*, Mike Fry[a], Ben Jackson[a], Leandro Bolzoni[b]

[a]TiDA Ltd, Toi Ohomai Institute of Technology, Tauranga, New Zealand
[b]Waikato Centre for Advanced Materials (WaiCAM), The University of Waikato, Hamilton, New Zealand

Received: November 28, 2018; Revised: May 22, 2019; Accepted: June 03, 2019

Selective laser melting (SLM) is an additive manufacturing technique which permits fabrication of three dimensional parts by selectively melting consecutive layers of metallic powder. This allows the production of parts with high geometrical complexity. Titanium alloy Ti-6Al-4V (Ti64) is widely used in industry due to its high strength-to-mass ratio, corrosion resistance and biocompatibility. SLM increases the application range of Ti64 because of its flexibility for prototyping any part and its low material waste. Nitriding is a diffusion-based thermo-chemical treatment for interstitial hardening of the surface of Ti64 alloy products. This study characterized the fatigue behaviour of SLM-produced Ti64 nitrided and annealed bars in as-built and machined surface conditions. The surface of the SLM-produced Ti64 parts after gas nitriding showed high values of micro-hardness up to 550 HV just below the surface. Fatigue testing was performed to assess the materials fatigue strength and fractographic imaging was used to examine fracture surface and nitride layer characteristics. Nitriding was found to reduce the fatigue strength of the samples to a similar level irrespective of being in the as-built or machined condition. The effect of nitriding on crack initiation and growth at various stress levels under fatigue loading was investigated.

Keywords: *Selective laser melting, Titanium, Fatigue, Gas nitriding, Crack initiation.*

1. Introduction

Selective Laser Melting (SLM), is an established technique in additive manufacturing (AM). SLM uses a high-power laser beam to fully melt powdered material placed on a flat surface, layer-by layer, to build three dimensional solid models with high density and usefully high mechanical properties[1-3]. The SLM process has been widely studied for different metallic powders, including: steels, titanium, nickel, tungsten, aluminium and copper alloys/composites[4-10]. Applications for SLM products include high value-added industries, such as medical, aerospace and automotive industries[1,11,12]. The combination of low density, good mechanical properties, corrosion resistance, fatigue resistance, high temperature performance, and biocompatibility makes titanium alloys using SLM, one of the most desirable material/manufacturing process combinations in the aerospace and biomedical fields[13-15].

Titanium nitriding is a process causing new phase formation on the surface of the material with a high hardness and a diffusion hardened zone beneath. It is one of the most popular thermo-chemical treatments to improve the tribological properties of Ti alloys. Nitriding of SLM-produced Ti64 alloy has been studied in the past and determined a surface TiN phase was present with α(N)-Ti interstitial hardening of the subsurface also examined[16].

Fatigue characterization of Ti alloys produced by AM[17-25] has also been widely investigated and data on fatigue life revealed important variability for a given applied stress[19]. The fracture toughness in SLM-produced Ti64 parts was found to be higher when the specimen notch was oriented perpendicular to the build layers. At low stress ratios, the crack growth rates were faster than in wrought titanium but became comparable at higher ratios[17]. Hot isostatic pressing (HIP) significantly improved the fatigue properties of SLM manufactured Ti64 material. Internal fatigue crack initiation was observed in very high cycle fatigue regimes as well as surface fatigue crack initiation from surface defects[18]. Ti64 samples produced by AM technique showed a significant improvement of ductility and fatigue strength by reduction of porosity using HIP[20] and improved fracture toughness values with a high temperature heat treatment[22].

Charkaluk observed three types of defect for the additively manufactured Ti64 parts: surface defects, un-melted zones, and small internal defects[24]. HIP treatment improved fatigue strength by decreasing the defects size, while the manufacturing direction was found to influence the presence of un-melted zones. Leuders et al.[26,27] studied post-process treatment effects on fatigue resistance and reported that SLM-produced Ti64 had an extended crack initiation phase, achieved by reducing

*e-mail: aamir.mukhtar@tida.co.nz

the porosity, which lead to a significant improvement in fatigue strength[26]. Under cyclic loading, SLM-produced Ti64 benefitted from HIP at a temperature of 920 °C.[27]. Yavari et al. studied the fatigue behaviour of porous Ti64 structures with different porosity levels manufactured using SLM and reported that S-N curves of porous structures with higher porosities were found to be lower than those with lower porosities[28]. Recently, fatigue crack propagation behaviour was examined for the SLM-produced porous Ti64 biomaterials with porosities between 66% and 84%, using compact-tension specimens[29].

Nitriding of titanium alloys is widely employed to improve wear resistance and surface hardness. As such its influence on fatigue properties for critical applications is important. The fatigue behaviour of gas-nitrided Ti64 alloy was found to have reduced fatigue life compared to those of the corresponding annealed material. The fatigue limit was however, improved slightly under certain nitriding conditions. The reduction in fatigue strength of the nitrided material was primarily attributed to premature crack initiation in the nitrided layer[30,31].

This present study aims to add to previous work by investigating how gas nitriding affects the fatigue properties of Ti64 manufactured using the SLM technique. Comparisons were made using samples in both nitrided and annealed states, with as-built and machined surface conditions. Specifically, the nature of cracks formed under fatigue conditions will be examined to understand how differences in fatigue failure might occur.

2. Experimental Procedure

All Ti64 samples were fabricated using SLM on an EOS M270 Machine. The machine was equipped with a Nd:YAG laser with a maximum power of 200 W. The SLM process was carried out in a closed chamber purged with argon gas to reduce the oxygen level to <0.1%. Parts were made from gas atomised, spherical Ti64 powder sourced from FalconTech Co. Ltd. meeting Titanium Grade 23 specification. This had a particle size distribution of 15µm (d_{10}) and 45µm (d_{90}), obtained using a laser diffraction particle size analyser (Analysette 22 Microtechplus, Fritsch). Samples were built in a vertical (Z axis) orientation in the SLM machine, generally considered as a worse case for properties, and avoided surface finish of the test section being influenced by the support material that would be required with horizontal built specimens. All samples were circular cross section. Rotating bend fatigue (RBF) specimens were "hour glass" form as shown in Fig. 1 with 5mm diameter at the minimum section.

Samples were tested in as-built and machined conditions to see if surface finish influenced fatigue performance. As-built specimens were manufactured at nominal test diameter while machined specimens were printed with 1mm increased diameter and machined to nominal test diameter.

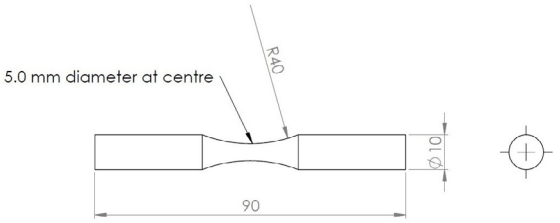

Figure 1. Nominal RBF sample geometry for SLM-produced Ti64.

Machining was undertaken on a CNC lathe in a commercial machine shop. Surface finish of the machined specimens was approximately R_a = 3 to 6 µm while the as-built surface was around R_a < 15 µm.

The as-built and machined, SLM-produced Ti64 bars were gas nitrided or annealed following the procedure outlined in Table 1. These treatments were carried out using a vacuum sintering furnace with heating performed at a rate of 10 °C/min and natural furnace cooling after the treatment time. High purity nitrogen gas was introduced with a fully controlled gas flow regulator (Vögtlin Instruments). Vickers microhardness measurements were used to identify the case depth of the nitride layer with a load of 50 g and a loading duration of 10 s.

Table 1. Method of vacuum furnace thermal treatment trials for Ti64 bars produced by SLM.

Process	Process Temperature	Time at process temperature	Atmosphere
	ºC	*hours*	
Annealing	850	4	Argon
Nitriding	850	4	Nitrogen[17]

Fatigue testing was performed on an in-house developed rotating bend fatigue testing machine based on Wöhler cantilever arrangement at 50 Hz rotation frequency. Two different samples that failed at different applied stress were selected for each condition to investigate residual fatigue cracks. The selected fatigue sample conditions and fatigue life for each are presented in Table 2.

Preparation for analysis of these residual cracks in the failed fatigue samples was performed by sectioning length-ways with an abrasive cutter (AbrasiMatic 300). This was followed by mounting and polishing the specimen to reveal any fatigue-initiated cracks along the samples length. Imaging (Zeiss EVO MA25 scanning electron microscope (SEM)) was used to examine the cross sections and measurements were recorded for crack length and location of crack with respect to fracture site. Fig. 2 shows SEM cross section micrographs of fatigue sample and some typical crack sites for SLM-produced Ti64 RBF nitrided specimen. Using this method cracks longer than 2µm could be accurately characterised.

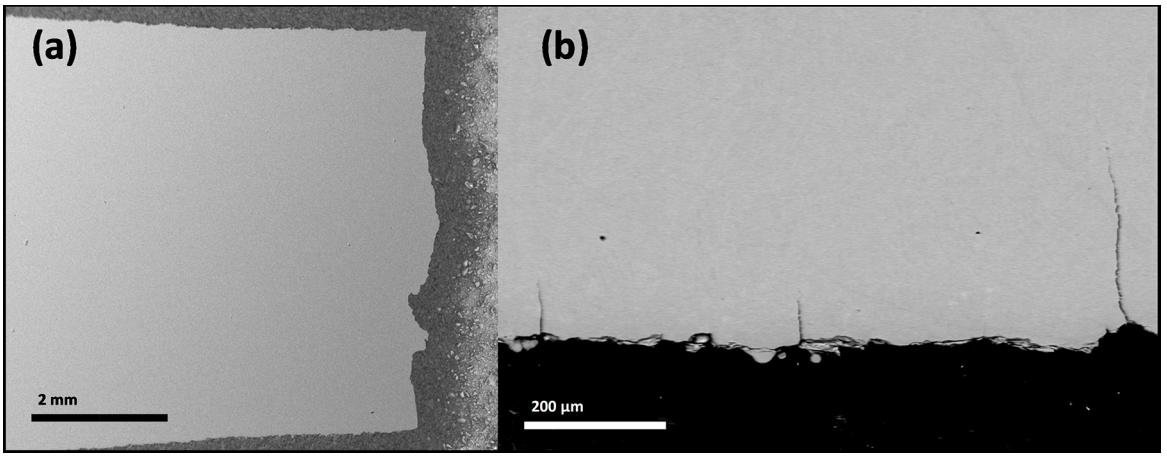

Figure 2. (a) Cross section micrograph of the fatigue fracture surface and (b) backscattered image of some crack sites for sectioned and prepared SLM-produced Ti64 RBF specimen.

Table 2. Summary of fatigue samples sectioned and investigated for residual cracks.

Specimen	Surface condition	Nominal stress	Cycles to failure
		MPa	*×10³*
Nitrided (N)	As-Built (AB)	255	161
		493	14
	Machined (M)	294	259
		502	12
Annealed (A)	As-Built (AB)	300	202
		487	21
	Machined (M)	407	61
		485	58

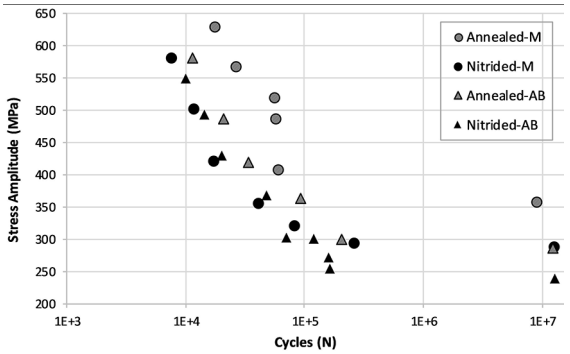

Figure 3. S-N curves for RBF of SLM-produced Ti64 material with machined and as-built surface, comparing nitrided and annealed conditions.

3. Results and Discussion

To evaluate the high-cycle-fatigue behaviour, RBF tests were conducted on SLM-produced as-built (AB) and machined (M) samples in nitrided and annealed condition. All fatigue tests were carried out at different stress amplitudes to explore fatigue lives comprising between 10^4 and 10^7 cycles. Tests were terminated at 10^7 cycles with this regarded as runout and the fatigue limit of the material. Fig. 3 shows the S-N curves of nitrided and annealed specimens in the different surface conditions. The fatigue limit in the nitrided condition AB and M specimens was 240 MPa and 287 MPa respectively. In the annealed condition machining improved the fatigue limit to 355 MPa compared to 285 MPa in the as-built material. Machining the surface of SLM-produced Ti64 in annealed condition improved the fatigue life while no clear benefit from machining was seen with the nitrided specimens. This suggests that nitriding may act as a crack initiation feature that acts to level the effect of other surface geometry concentrating factors.

Fig. 4 (a) and (b) present the number of cracks and average crack length for each of the specimens. Low and high designation in the sample labels are given to note the nominal stress level for the sample (Table 2). In both annealed and nitrided samples there was a greater number of residual cracks in the higher stress samples. This is expected due to the greater stress enabling crack initiation. Across all the samples there is no overall difference in the number of cracks between nitriding and annealing. Annealing shows reduced number of cracks in the machined samples which is not the case for the nitrided ones. This supports the fatigue life data where the surface geometry in nitrided samples had little effect on the performance of the material.

Average crack length is also found to be longer in the high stressed samples. A higher stress increases the rate of crack propagation so combined with increased crack initiation the average crack length is expected to be greater. This is especially evident in the nitrided material. Significantly, the average crack length of the nitrided samples was considerably greater than that of the annealed material despite similarities in the number of cracks observed. This suggests that through nitriding, a larger proportion of cracks were enabled to grow to greater lengths as a result of earlier initiation of crack or faster crack propagation.

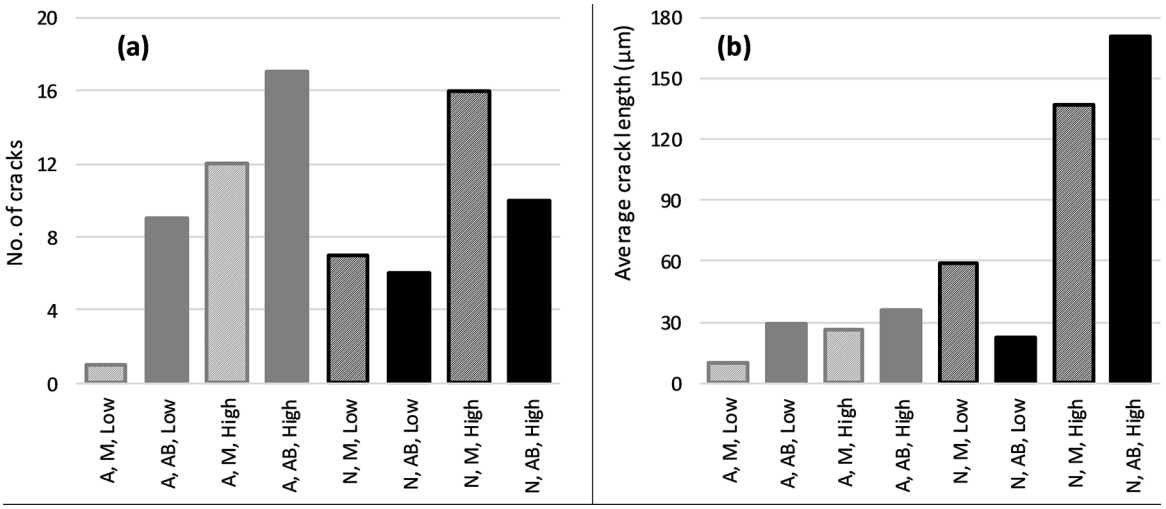

Figure 4. (a) Number of cracks and (b) average crack length for the sectioned RBF samples. (See Table 2 for samples' condition details).

Crack length is plotted against local stress for each crack observed in the RBF samples and the results are shown in Fig. 5 (a) for nitrided samples and Fig. 5 (b) for annealed samples. Local stress was calculated allowing for a difference in bending moment and specimen diameter at the location of the individual crack.

In the nitrided samples (Fig. 5 (a)) there is an evident increase in maximum observed crack length for an increase in applied stress. At higher stress cracks were present at lengths between 40 µm and 300 µm with an even distribution throughout that range. At low stress levels cracks were observed to be much smaller not exceeding 105 µm. As-built

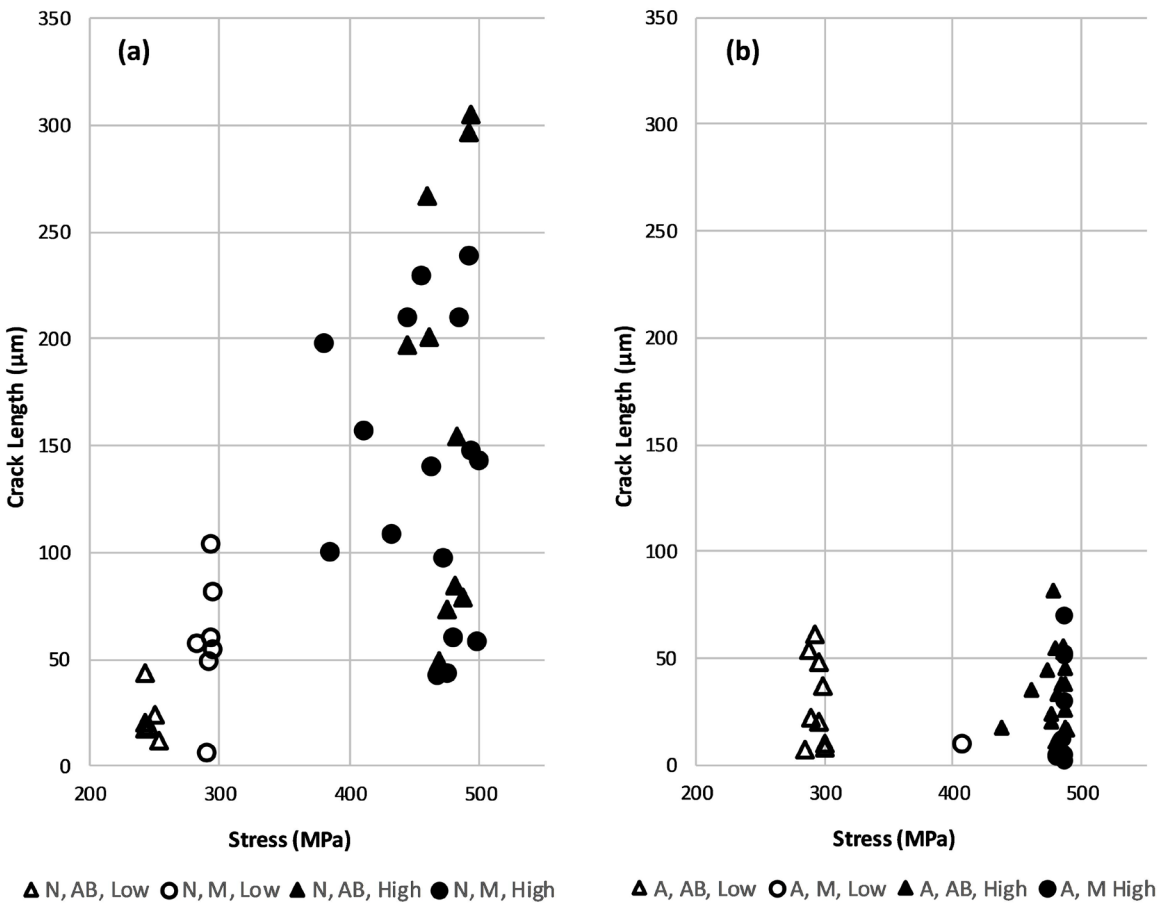

Figure 5. Local stress at each crack site vs crack length for (a) nitrided and (b) annealed RBF samples in different surface conditions.

samples appeared to have longer residual cracks than those present in the machined material, due to the easier crack initiation in the rougher surface allowing more time for the crack to grow. The nitrided, machined material at low stress appeared to have longer cracks than the as-built material. This difference could be due to the samples having been tested at a slightly higher stress (294 MPa compared to 255 MPa) which may account for this difference.

The annealed samples (Fig. 5 (b)) showed maximum crack lengths far below those of the nitrided material, not exceeding 82 µm. Again, the higher stressed sample displayed longer cracks however this was not as pronounced as in the nitrided condition. As-built samples also had the maximum residual crack length, however this was not significantly greater than the machined samples. In the samples investigated, minimum cracks less than 10 µm were present in all cases which was different to the higher stress levels in the nitrided material.

To try and explain the difference in crack length and reduced fatigue life of the nitrided material, the case depth of the nitride layer was investigated through microhardness as shown in Fig. 6. The nitriding process is a diffusion-based mechanism which generates a reducing hardness profile into the material. The hardness reduced from 550 HV just below the surface of the nitrided samples to the bulk Ti64 hardness of 350 HV at a depth of 30 µm from the surface. In nitrided samples the cracks at high stress were no shorter than 45 µm (Fig. 5 (a)). The minimum observed crack was greater than the thickness of the nitride layer. This suggests that cracks may propagate through the nitride layer very rapidly, so crack lengths will always be greater than the nitrided layer and as such no short length cracks were observed to be present. The cracks in the annealed samples support this as there are short cracks present when subject to high stress.

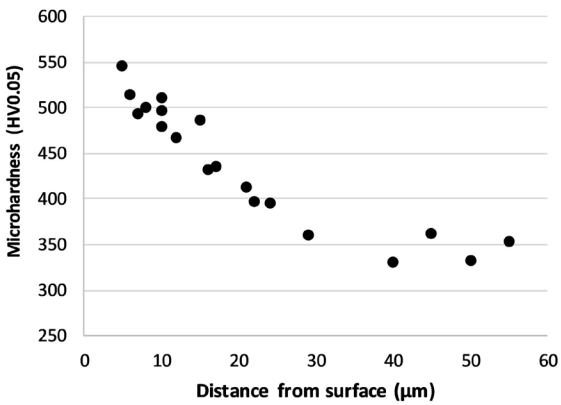

Figure 6. Hardness measurements indicating the thickness of the nitride layer. Measurements taken from a sectioned Ti64 RBF sample with machined then nitrided surface.

At lower stress in the nitrided material, cracks were present which were shorter than the thickness of the nitrided layer. The cracks in this case either initiated later in the fatigue test or did not experience the same propagation rate through the nitride layer seen at high stress. Because of this these cracks remain short.

For a crack to grow it must be above the threshold stress for the material. Because the cracks initiate and grow rapidly through the nitride layer at higher stress, when they reach the bulk material the cracks are now sufficiently long to continue to grow. Because of Paris's law this will result in the cracks having a high stress intensity, and as such, a higher growth rate into the centre of the fatigue samples. The cracks observed in the nitrided material were longer than those of the annealed samples due to this fast growth through the nitride layer and consequently faster growth rate through the bulk material. The annealed samples didn't experience this initial rapid growth rate and as such propagated much more slowly.

Different cracks that formed in the nitrided material under fatigue are presented in Fig. 7. This shows cracks parallel to the surface at a depth of less than 20 µm, putting them within the nitrided layer. Nitrogen is known to reduce toughness and embrittle titanium so being subject to a higher bending moment and subsequent high stress at the surface could cause the nitrided layer to fracture in this way, separating from the substrate material. These parallel cracks were not included in the count of fatigue cracks. A classic fatigue crack propagating perpendicular to the surface into the material is also shown in Fig. 7 highlighting the difference between surface and fatigue cracking.

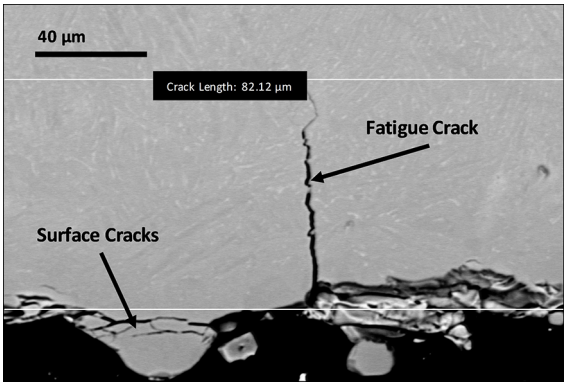

Figure 7. Cross section image of the surface of an as-built, nitrided, RBF sample showing different crack features. Surface cracks running parallel to the fatigue samples surface as well as a perpendicular fatigue crack into the bulk material.

For the observations made in these samples there are limitations. The cracks observed are not necessarily the actual maximum crack length as the section could be taken through one side of the crack thus understating its length. This is possibly the case with the annealed, machined sample at lower stress. Only one crack was observed in this sample.

If the section were taken at a different orientation, different cracks may have been observed. This data only

serves to understate the number of cracks and crack lengths so serves as a conservative lower boundary compared to the real effects. The crack that causes failure is always the longest crack, so the maximum length of crack observed here must not be taken as the critical crack length.

4. Conclusions

Nitriding was shown to reduce the fatigue life of AM Ti64 compared to AM Ti64 subject to the same thermal treatment without nitriding. This can be attributed to the brittle nitrided layer that allowed early crack initiation, rapid crack propagation through to the bulk material as well as faster growth rate of these cracks.

At lower stress this effect was less pronounced as there were similar crack lengths in the annealed material. There were also cracks at lengths that placed them within the nitrided layer.

There was evidence that the nitride layer suffered some delamination with cracks running parallel to the surface present at a depth still within the hardened coating.

5. Acknowledgments

The authors want to acknowledge the financial support from New Zealand Ministry of Business, Innovation and Employment (MBIE) through the TiTeNZ (Titanium Technologies New Zealand) research contract.

6. References

1. Yap CY, Chua CK, Dong ZL, Liu ZH, Zhang DQ, Loh LE, et al. Review of selective laser melting: Materials and Applications. *Applied Physics Reviews*. 2015;2(4):041101.

2. Van Hooreweder B, Kruth JP. Advanced fatigue analysis of metal lattice structures produced by Selective Laser Melting. *CIRP Annals*. 2017;66(1):221-224.

3. Wei C, Li L, Zhang X, Chueh YH. 3D printing of multiple metallic materials via modified selective laser melting. *CIRP Annals*. 2018;67(1):245-248.

4. Ivekovic A, Omidvari N, Vrancken B, Lietaert K, Thijs L, Vanmeensel K, et al. Selective laser melting of tungsten and tungsten alloys. *International Journal of Refractory Metals & Hard Materials*. 2018;72:27-32.

5. Kruth JP, Froyen L, Van Vaerenbergh J, Mercelis P, Rombouts M, Lauwers B. Selective laser melting of iron-based powder. *Journal of Materials Processing Technology*. 2004;149(1-3):616-622.

6. Thijs L, Verhaeghe F, Craeghs T, Van Humbeeck J, Kruth JP. A study of the microstructural evolution during selective laser melting of Ti-6Al-4V. *Acta Materialia*. 2010;58(9):3303-3312.

7. Song B, Dong S, Zhang B, Liao H, Coddet C. Effects of processing parameters on microstructure and mechanical property of selective laser melted Ti6Al4V. *Materials & Design*. 2012;35:120-125.

8. Amato KN, Gaytan SM, Murr LE, Martinez E, Shindo PW, Hernandez J, et al. Microstructures and mechanical behaviour of Inconel 718 fabricated by selective laser melting. *Acta Materialia*. 2012;60(5):2229-2239.

9. Li R, Shi Y, Wang Z, Wang L, Liu J, Jiang W. Densification behaviour of gas and water atomized 316L stainless steel powder during selective laser melting. *Applied Surface Science*. 2010;256(13):4350-4356.

10. Dai D, Gu D. Thermal behaviour and densification mechanism during selective laser melting of copper matrix composites: Simulation and experiments. *Materials & Design*. 2014;55:482-491.

11. Yadroitsev I, Krakhmalev P, Yadroitsava I. Selective laser melting of Ti6Al4V alloy for biomedical applications: Temperature monitoring and microstructural evolution. *Journal of Alloys and Compounds*. 2014;583:404-409.

12. Boyer RR. An overview on the use of titanium in the aerospace industry. *Materials Science and Engineering: A*. 1996;213(1-2):103-114.

13. Murr LE, Quinones SA, Gaytan SM, Lopez MI, Rodela A, Martinez EY, et al. Microstructure and mechanical behaviour of Ti-6Al-4V produced by rapid-layer manufacturing, for biomedical applications. *Journal of the Mechanical Behaviour of Biomedical Materials*. 2009;2(1):20-32.

14. Kumar P, Prakash O, Ramamurty U. Micro-and meso-structures and their influence on mechanical properties of selectively laser melted Ti-6Al-4V. *Acta Materialia*. 2018;154:246-260.

15. Zhang H, Zhao J, Liu J, Qin H, Ren Z, Doll GL, et al. The effects of electrically-assisted ultrasonic nanocrystal surface modification on 3D-printed Ti-6Al-4V alloy. *Additive Manufacturing*. 2018;22:60-68.

16. Franz P, Mukhtar A, Downing W, Smith G, Jackson B. Mechanical Behaviour of Gas Nitrided Ti6Al4V Bars Produced by Selective Laser Melting. *Key Engineering Materials*. 2016;704:225-234.

17. Edwards P, Ramulu M. Effect of build direction on the fracture toughness and fatigue crack growth in selective laser melted Ti-6Al-4V. *Fatigue & Fracture of Engineering Materials & Structures*. 2015;38(10):1228-1236.

18. Günther J, Krewerth D, Lippmann T, Leuders S, Tröster T, Weidner A, et al. Fatigue life of additively manufactured Ti-6Al-4V in the very high cycle fatigue regime. *International Journal of Fatigue*. 2017;94(Pt 2):236-245.

19. Li P, Warner DH, Fatemi A, Phan N. Critical assessment of the fatigue performance of additively manufactured Ti-6Al-4V and perspective for future research. *International Journal of Fatigue*. 2016;85:130-143.

20. Kasperovich G, Hausmann J. Improvement of fatigue resistance and ductility of TiAl6V4 processed by selective laser melting. *Journal of Materials Processing Technology*. 2015;220:202-214.

21. Nicoletto G. Anisotropic high cycle fatigue behaviour of Ti-6Al-4V obtained by powder bed laser fusion. *International Journal of Fatigue*. 2017;94(Pt 2):255-262.

22. Greitemeier D, Palm F, Syassen F, Melz T. Fatigue performance of additive manufactured TiAl6V4 using electron and laser beam melting. *International Journal of Fatigue*. 2017;94(Pt 2):211-217.

23. Zhao S, Li SJ, Wang SG, Hou WT, Li Y, Zhang LC, et al. Compressive and fatigue behaviour of functionally graded Ti-6Al-4V meshes fabricated by electron beam melting. *Acta Materialia*. 2018;150:1-15.

24. Chastand V, Quaegebeur P, Maia W, Charkaluk E. Comparative study of fatigue properties of Ti-6Al-4V specimens built by electron beam melting (EBM) and selective laser melting (SLM). *Materials Characterization*. 2018;143:76-81.

25. Wu Y, Bao R. Fatigue crack tip strain evolution and crack growth prediction under single overload in laser melting deposited Ti-6.5Al-3.5Mo-1.5Zr-0.3Si titanium alloy. *International Journal of Fatigue*. 2018;116:462-472.

26. Leuders S, Thöne M, Riemer A, Niendorf T, Tröster T, Richard HA, et al. On the mechanical behaviour of titanium alloy TiAl6V4 manufactured by selective laser melting: Fatigue resistance and crack growth performance. *International Journal of Fatigue*. 2013;48:300-307.

27. Leuders S, Lieneke T, Lammers S, Tröster T, Niendorf T. On the fatigue properties of metals manufactured by selective laser melting - The role of ductility. *Journal of Materials Research*. 2014;29(17):1911-1919.

28. Yavari SA, Wauthle R, van der Stoke J, Riemslag AC, Janssen M, Mulier M, et al. Fatigue behaviour of porous biomaterials manufactured using selective laser melting. *Materials Science and Engineering: C*. 2013;33(8):4849-4858.

29. Hedayati R, Yavari SA, Zadpoor AA. Fatigue crack propagation in additively manufactured porous biomaterials. *Materials Science and Engineering: C*. 2017;76:457-463.

30. Shibata H, Tokaji K, Ogawa T, Hori C. The effect of gas nitriding on fatigue behaviour in titanium alloys. *International Journal of Fatigue*. 1994;16(6):370-376.

31. Tokaji K, Ogawa T, Shibata H, Kamiya Y. Effect of Gas Nitriding on Fatigue Behaviour of Ti6Al4V Alloy. *Transactions of the Japan Society of Mechanical Engineers, Part A*. 1991;57(542):2293-2299.